Electrochimica Acta 470 (2023) 143342

Contents lists available at ScienceDirect

Electrochimica Acta

journal homepage: www.journals.elsevier.com/electrochimica-acta

Synergistically coupling of trimetallic sulfides on Ni foam as porous self-supported electrodes for alkaline water splitting

Rong He [a], Pitchai Thangasamy [a], Junlin Wu [b], Kunpeng Yu [c], Xiaolu Yu [b], Wei Tang [c], Devon Quiroz [a], Deema Alyones [a], Zheng Chen [c], Hongmei Luo [a], Meng Zhou [a,*]

[a] Department of Chemical & Materials Engineering, New Mexico State University, Las Cruces, NM 88003, USA
[b] Program of Materials Science and Engineering, University of California, San Diego, La Jolla, CA 92093, USA
[c] Department of NanoEngineering, University of California San Diego, La Jolla, CA 92093, USA

ARTICLE INFO

Keywords:
Alkaline water splitting
Trimetallic sulfides
Self-supported catalysts
OER
HER

ABSTRACT

The development of highly active, highly durable, and inexpensive electrode materials for water electrolysis is essential for future sustainable energy systems. Herein, we demonstrate heterostructures of metal sulfides deposited on Ni foam (NF) through electrodeposition for highly efficient water splitting. Iron-cobalt-nickel sulfides deposited on Ni foam (FeCoNiS@NF) exhibit a low overpotential of 302 mV (at 50 mA cm^{-2}) for OER, and molybdenum-cobalt-nickel sulfides on Ni foam (MoCoNiS@NF) can provide a current density of 10 mA cm^{-2} at an overpotential of 114 mV for HER in alkaline solution. The lower charge-transfer resistance and Tafel slope values for FeCoNiS@NF and MoCoNiS@NF electrodes demonstrate the favorable reaction kinetics toward OER and HER, respectively, resulting from their intrinsic catalytic activity, good electrical conductivity, and accessible active sites. Furthermore, FeCoNiS@NF as anode and MoCoNiS@NF as cathode require a cell voltage of 1.68 V to produce a current density of 10 mA cm^{-2} with impressive durability under alkaline conditions, further proving the advancement and potential of trimetallic sulfides with optimal interfaces in the development of cost-effective electrodes for alkaline water splitting.

1. Introduction

Green hydrogen has attracted widespread attention thanks to its high gravimetric energy density and the potential to deal with environmental pollution threats and fossil fuel depletion [1–3]. Electrochemical water splitting provides us with a reliable pathway to producing clean hydrogen from renewable sources [4–6]. In an alkaline solution, water splitting involves a cathodic hydrogen evolution reaction (HER: $2H_2O + 2e^- \rightarrow H_2 + 2OH^-$) and an anodic oxygen evolution reaction (OER: $4OH^- \rightarrow O_2 + 2H_2O + 4e^-$) [7]. The theoretical potential of water splitting is 1.23 V [7]. However, it usually requires a much higher operating cell voltage to achieve the desired current density due to its kinetically sluggish process. HER and OER are significantly influenced by electrocatalysts. Currently, noble metal materials such as Pt, Ir, and Ru-based electrocatalysts are employed as commercial electrodes for HER and OER, owing to their excellent electrocatalytic activities [8–10]. The excessive price and rare nature of these precious metal-based materials hamper their application in industrial-scale water electrolysis systems. Exploring low-cost, highly active, and durable electrocatalysts is demanding and still faces tough challenges. Transition metal-based materials present their advantages of high earth abundance and low cost, which have been intensely studied as electroactive materials for electrochemical applications and could be promising alternative electrocatalysts for HER and OER [11–16]. So far, these nonprecious materials such as transition-metal hydroxides, oxides, chalcogenides, phosphides, and alloys have shown their promising electrocatalytic activities toward HER and OER [4,17-20]. In the fabrication of electrodes for HER and OER, the typical approach is to make an electrocatalyst slurry where the active material, a conductive compound, and a binder are mixed in a suitable solvent and then dropped onto the conductive substrate. The existence of a binder may cause high resistance for the electrode and thus affect its electrochemical activity [21]. It may also affect the electrode stability, especially operating at a high current density, resulting from the stripping of active materials from the electrode. These challenges inspire more and more researchers to develop binder-free electrocatalysts. Enormous efforts have been devoted to

* Corresponding author.
E-mail address: mzhou@nmsu.edu (M. Zhou).

https://doi.org/10.1016/j.electacta.2023.143342
Received 7 July 2023; Received in revised form 3 October 2023; Accepted 10 October 2023
Available online 11 October 2023

growing or depositing active materials on different substrates such as copper foil, titanium foil, nickel foam, and carbon cloth/paper by several synthetic approaches [22–24]. For instance, Wang et al. synthesized NiCoP@NiMn-based electrocatalysts via a hydrothermal process [25]. This electrocatalyst is simultaneously highly active toward HER and OER. They concluded some advantages of this electrocatalyst: (1) high intrinsic activity; (2) good electrical conductivity; and (3) Ni foam with a large surface area for active sites and 3D structure for the release of gas bubbles [25].

Transition metal sulfides have been widely utilized in alkaline water electrolysis systems, thanks to their high electrical conductivity and excellent intrinsic activity [26–28]. Several transition metal sulfides have been demonstrated as efficient electrocatalysts for OER (e.g., Co_xS_y, Ni_xS_y, Fe_xS_y, and Cu_xS_y) and HER (e.g., Co_xS_y, Ni_xS_y, W_xS_y, and MoS_2) [29–34]. Zheng et al. reported a polyol solution method to prepare nickel sulfide catalysts with different phases and demonstrated that Ni_3S_2 has better water-splitting performance compared with NiS and NiS_2. They pointed out that the good catalytic activity of Ni_3S_2 is owing to the abundant active centers, high metallic conductivity, and optimal Gibbs free energy for catalyst-H* for HER [35]. Binary metal sulfides have also been explored for water-splitting reactions in alkaline media [33,36]. It was reported that Ni_3S_2/FeS showed higher HER and OER activities than single metal sulfides (Ni_3S_2 and FeS) [37]. The corresponding DFT calculations revealed that the H^+ and OH^-adsorption is more favorable for Ni_3S_2/FeS interfaces compared with Ni_3S_2 and FeS, resulting from its lower adsorption energy [37]. This result also indicated that the synergistic effect of different metal sulfides could change the intrinsic electronic structures and adsorption energy thus exposing more accessible active sites and improving the catalytic activities for electrochemical reactions during the water-splitting process. The above results imply that the design of multi-transition-metal sulfide electrocatalysts effectively improves the water-splitting performance of non-precious electrocatalysts. However, as far as we know, trimetallic sulfides in alkaline water splitting for H_2 production are relatively less studied. Their corresponding working mechanisms are still unclear and need further exploration.

Herein, we report the preparation of heterostructure trimetallic sulfides on Ni foam substrates as porous self-supported electrodes for OER and HER via an energy-saving electrodeposition process. FeCoNiS@NF presents a low overpotential of 302 mV (at 50 mA cm^{-2}) during the OER process, and MoCoNiS@NF only requires an overpotential of 114 mV to achieve a current density of 10 mA cm^{-2} for HER. The desirable OER and HER activities of the trimetallic sulfides result from the synergistic effect of heterostructure interfaces of multi-metal sulfides, providing high intrinsic catalytic activity and a large amount of catalytic active sites. The fast reaction kinetics of trimetallic sulfides were confirmed by observing lower charge-transfer resistance and Tafel slopes.

Importantly, we demonstrated an efficient synergistic strategy for enhancing OER/HER performances by incorporating Fe/Mo to cobalt-nickel sulfides. The FeCoNiS@NF/ MoCoNiS@NF present good water-splitting activity and durability, which could be promising electrodes to alternative noble metal-based materials for alkaline water electrolysis. This work also provides valuable insights into the working mechanisms behind the OER/HER catalytic process based on Tafel slope and electrochemical impedance spectroscopy analysis.

2. Experimental section

2.1. Chemicals

Nickel nitrate hexahydrate ($Ni(NO_3)_2{\cdot}6H_2O$, 97.0%), cobalt nitrate hexahydrate ($Co(NO_3)_2{\cdot}6H_2O$, 98.0%), Iron chloride hexahydrate ($FeCl_3{\cdot}6H_2O$, 98.0%), sodium molybdate dihydrate ($Na_2MoO_4{\cdot}2H_2O$, 99.5%), hydrochloric acid (HCl), thiourea, potassium hydroxide (KOH), iridium oxide (IrO_2) powder, 20% platinum on graphitized carbon (Pt/C), and ethanol were obtained from Sigma-Aldrich. The above chemicals were used without further treatment.

2.2. Electrocatalyst synthesis

Metal sulfides deposited on Ni foam electrodes were fabricated by an electrodeposition method, which is schematically shown in **Figure S1**. Briefly, Ni foam substrates were pre-treated by ultrasonication in acid (3 M HCl), deionized (DI) water, and ethanol sequentially to clean the Ni foam surface. Then, the treated Ni foam substrates were placed in a vacuum oven (60 °C) for dying. The electrodeposition was conducted in a three-electrode cell using a piece of Ni foam (1 × 1 cm^2) as the working electrode. A graphite rod and silver/silver chloride (Ag/AgCl) served as the counter and reference electrodes, respectively. 1.5 mmol Ni $(NO_3)_2{\cdot}6H_2O$ and 0.05 mol thiourea in 50 mL DI water were employed as the electrolyte to achieve the NiS@NF self-standing electrode. Whereas 0.75 mmol $Co(NO_3)_2{\cdot}6H_2O$, 0.75 mmol $Ni(NO_3)_2{\cdot}6H_2O$, and 0.05 mol thiourea were used to deposit the bimetallic sulfides (CoNiS@NF) on the Ni foam substrate. Finally, trimetallic sulfides were grown on the Ni foam substrate (FeCoNiS@NF/MoCoNiS@NF) using 0.5 mmol $Co(NO_3)_2{\cdot}6H_2O$, 0.5 mmol $Ni(NO_3)_2{\cdot}6H_2O$, 0.05 mol thiourea and 0.5 mmol $FeCl_3{\cdot}6H_2O$/$Na_2MoO_4{\cdot}2H_2O$ precursors. The electrodeposition process was performed with a potential of −1.2 V (vs. Ag/AgCl) for 900 s in the corresponding electrolyte solution by chronoamperometry. After deposition, the as-prepared self-standing electrodes were rinsed several times with DI water and ethanol and then dried at 60 °C. The mass loadings of the fabricated NiS@NF, CoNiS@NF, FeCoNiS@NF, and MoCoNiS@NF were about 4.7 mg cm^{-2}, 4.2 mg cm^{-2}, 1.2 mg cm^{-2}, and 4.7 mg cm^{-2}, respectively.

2.3. Morphological and structural characterization

The field emission scanning electron microscopy (FESEM, Tescan Mira3) and energy dispersive X-ray spectroscopy (EDS) were carried out to analyze the morphology and elemental distribution of the synthesized catalysts. The structures of materials were further characterized by transmission electron microscopy (TEM, ThermoFisher Talos 200X). The structure of the prepared electrode materials was identified by powder X-ray diffraction (XRD) with a PANalytical Empyrean powder diffractometer. The compositions of deposited layers on the NF surface were characterized by Raman spectroscopy (excitation wavelength: 532 nm). X-ray photoelectron spectroscopy (XPS) was carried out using an AXIS Supra by Kratos Analytical equipped with an Al anode monochromatic X-ray source anode source at 15 kV with a 5.0 × 10–8 Torr vacuum level. All the peaks were fitted based on the reference C—C bond at 284.6 eV. The specific surface areas of the samples were determined by nitrogen adsorption−desorption tests (Micromeritics ASAP 2050) based on the Brunauer-Emmett-Teller (BET) theory.

2.4. Electrochemical measurements

All electrochemical tests of the electrodes were conducted using an electrochemical workstation (CHI 760C) in a three-electrode cell system in 1 M KOH solution. The as-fabricated electrodes (1 × 1 cm^2) were directly employed as the working electrode, while a graphite rod and a silver/silver chloride (Ag/ AgCl) were utilized as counter and reference electrodes, respectively. The measured potentials were converted to a reversible hydrogen electrode (RHE) potential: E (RHE) = E (Ag/AgCl) + 0.059 pH +0.205 V. To reach a stable condition, working electrodes were pre-cycled by cyclic voltammetry (CV, 10 mV s^{-1}). The polarization curves were measured from linear sweep voltammetry (LSV, 5 mV s^{-1}). Electrochemical impedance spectroscopy (EIS) was performed with a frequency range from 10^5 Hz to 0.1 Hz. The electrode durability testing was conducted by chronopotentiometry (CP).

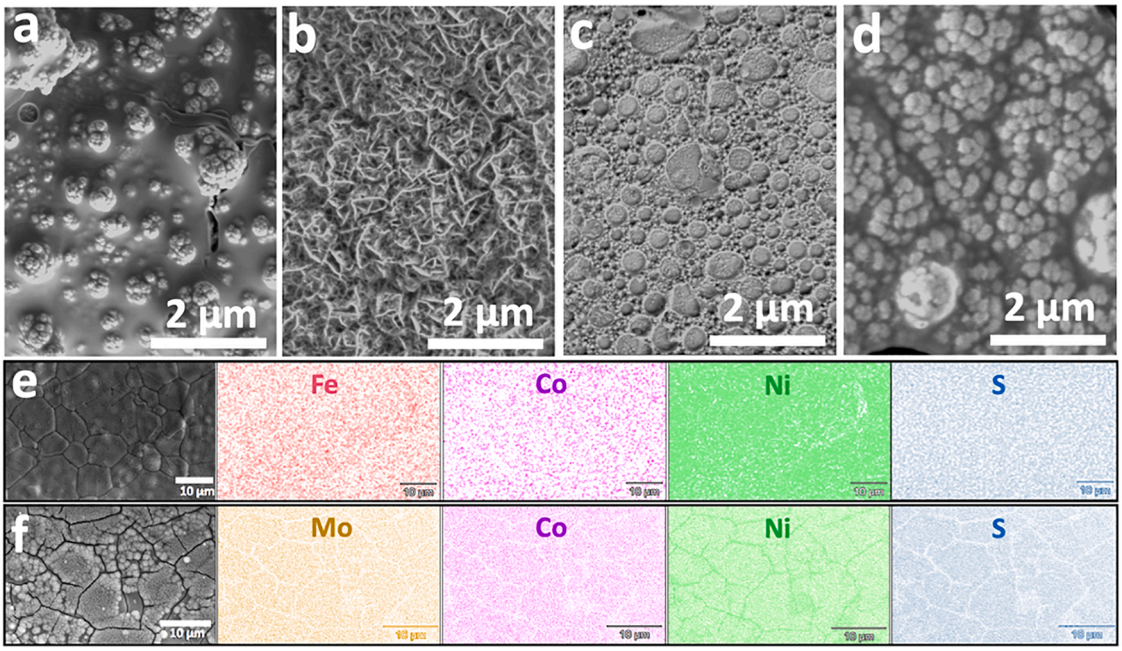

Fig. 1. SEM images of (a) NiS@NF, (b) CoNiS@NF, (c) FeCoNiS@NF, and (d) MoCoNiS@NF with different magnifications. The elemental mapping images of (e) FeCoNiS@NF and (f) MoCoNiS@NF.

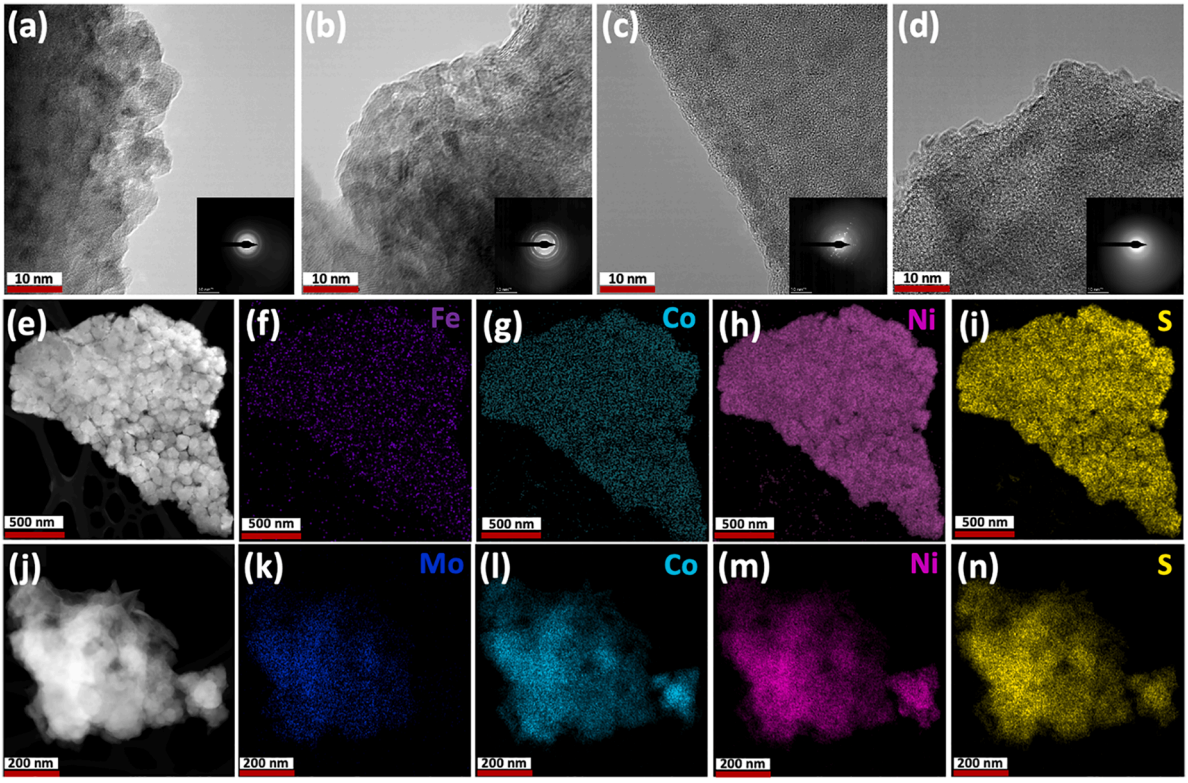

Fig. 2. TEM images and insert SAED patterns of (a) NiS@NF, (b) CoNiS@NF, (c) FeCoNiS@NF, and (d) MoCoNiS@NF; The corresponding elemental mappings of (e-i) FeCoNiS@NF and (j-n) MoCoNiS@NF.

3. Results and discussion

3.1. Characterization of electrodeposited self-standing electrodes

SEM images in Fig. 1 are illustrative of the morphologies of the various metal sulfides deposited on Ni foam by an electrodeposition process. Clearly, NiS@NF is composed of agglomerative nickel sulfide particles and presents a lumpy surface (Fig. 1**a**). Fig. 1**b** reveals that densely-packed cobalt-nickel sulfide nanoflakes were grown on Ni foam surface. It is interesting to note that the nano-architecture of cobalt-nickel sulfides changed drastically after the incorporation of Fe (Fig. 1**c**) and Mo (Fig. 1**d**), revealing that the nucleation and growth

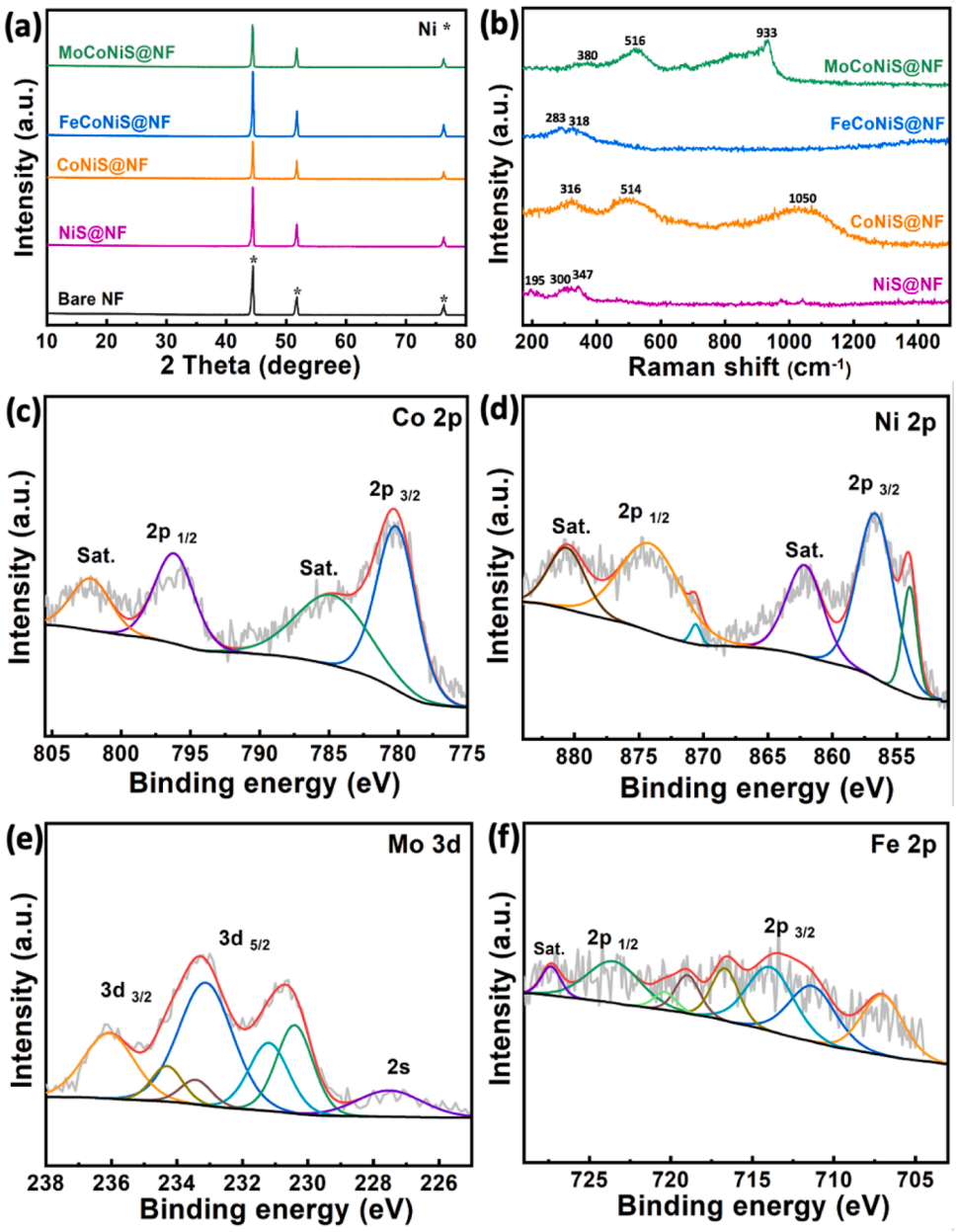

Fig. 3. (a) XRD patterns and (b) Raman spectra of different self-standing electrodes. High-resolution XPS spectrum of (c) Co 2p, (d) Ni 2p, (e) Mo 3d of MoCoNiS@NF, and (f) Fe 2p of FeCoNiS@NF.

process is greatly affected by the incorporation of third transition metal elements. The corresponding elemental mappings indicate that Fe/Mo, Co, Ni, and S atoms are well dispersed throughout the surface of FeCoNiS@NF/MoCoNiS@NF electrode (Figs. 1**e and** 1**f**), confirming the formation of multiple-metal sulfides on Ni foam.

TEM offers a closer observation of the electrode structures, providing information about the nanostructures of the materials [38,39]. As shown in Fig. 2**a**, the microstructure of NiS@NF is constructed by nanoparticles. The SAED pattern of NiS@NF (inset, Fig. 2**a**) reveals its amorphous nature, further supported by XRD results. The crystallinity of NiS@NF has been improved by the incorporation of Co (inset, Fig. 2**b**) and Co/Fe metal atoms (inset, Fig. 2**c**) due to the formation of Co- and Fe-based sulfides. While the incorporation of Mo metal atoms does not alter the crystallinity of NiS@NF as clearly seen in Fig. 2**d** (inset) [40]. Fig. 2**b-d** demonstrated the microstructure evolution of nickel sulfides after the incorporation of Co, Fe, and Mo. The homogeneous distribution of Fe/Mo, Co, Ni, and S atoms in FeCoNiS@NF/MoCoNiS@NF electrode was confirmed from SEM-EDS results (Fig. 2**e-n**). The elemental composition of different electrodes is shown in **Table S1**. These observations demonstrated the formation of monometallic (Ni), bimetallic (Co-Ni), and trimetallic (Fe-Co-Ni and Mo-Co-Ni) sulfides on Ni foam by electrodeposition process. The mass loading of each metal sulfide catalyst on Ni foam is less than 5 mg cm^{-2}, which is comparable with the self-standing Ni foam-based electrodes for electrochemical applications in the literature [41–43]. Ni foam-based electrodes exhibit different surface areas possibly depending on the active material structures and synthesis methods, which may affect their electrocatalytic activities during the electrochemical process [44,45]. The Brunauer–Emmett–Teller (BET) test was carried out to study the porous structures of different metal sulfides. N_2 adsorption-desorption isotherm curves of different electrodes are shown in **Figure S2**. The calculated BET surface area of bare NF is 2.45 m^2 g^{-1}, which is consistent with the results reported in the literature [46]. All the metal sulfide electrodes have a higher BET surface area (3.03 m^2 g^{-1} ~ 6.85 m^2 g^{-1}) than bare NF,

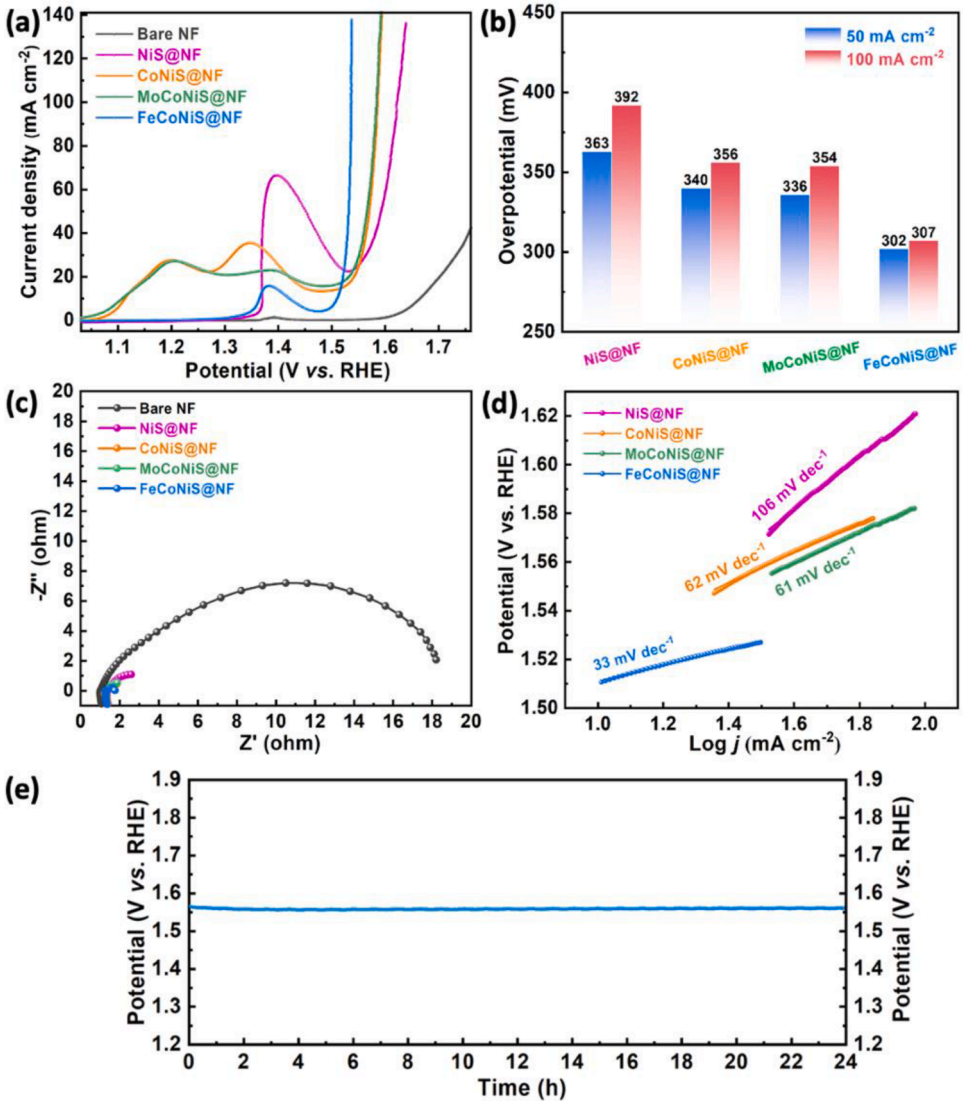

Fig. 4. (a) LSV in the oxygen-evolution regime for working electrodes; (b) comparison of overpotentials (after iR-correction) versus different materials for OER; (c) Nyquist plots determined at 1.58 V (vs. RHE).; (d) Tafel plots and (e) electrode durability of FeCoNiS@NF at 30 mA cm^{-2} (without iR-correction).

demonstrating an increase in electrode surface area due to the deposition of metal sulfides on NF.

XRD patterns of as-fabricated electrodes are presented in Fig. 3**a**. The characteristic Ni foam diffraction peaks were observed in all metal sulfide samples. The electrodeposited metal sulfides mono, bimetallic or trimetallic sulfides did not show any XRD peaks, probably due to the deposition of metal sulfides with amorphous properties. Therefore, Raman spectrometry was performed to analyze the structures of the as-synthesized metal sulfide materials (Fig. 3**b**). Raman spectrum of NiS@NF showed vibrational modes at 195, 300, and 347 cm^{-1}, which in agreement with the literature data corresponded to Ni_3S_2 [47]. A peak at 316 cm^{-1} was found for CoNiS@NF, corresponding to the S atoms toward the tetrahedral site Ni atom (S-Nitetra–S bonds) [48]. CoNiS@NF presents a peak at 514 cm^{-1}, indicating the Raman active modes and vibrations in ternary nickel cobalt sulfide ($NiCo_2S_4$) [48]. A broad peak around 1050 cm^{-1} is identified, which may be introduced by vulcanization [49]. These results indicate the formation of nickel-cobalt sulfides in as-synthesized CoNiS@NF by an electrodeposition process. FeCoNiS@NF has several minor peaks at 200–600 cm^{-1}, which may be attributed to the vibrations of FeS and $FeCoS_2$/ $FeNiS_2$, indicating the co-existence of different Fe-contained metal sulfides [50]. For MoCoNiS@NF, A peak at ~380 cm^{-1} may result from the stretching vibration of the MoS_x [51]. The peak of nickel-cobalt sulfides was also identified in MoCoNiS@NF spectra. Besides, the characteristic peak at ~ 933 cm^{-1} presents the $CoMoS_4$ Raman vibration [51]. These observations suggested that multilayered Mo-contained metal sulfides were successfully deposited on Ni foam in MoCoNiS@NF.

XPS analysis was conducted to further confirm their structures and elemental compositions. The XPS full-scan survey indicates the coexistence of Mo, Co, Ni, and S elements in MoCoNiS@NF. (**Figure S3a**). Fig. 3**c-e** analyzed the XPS spectra of Co 2p, Ni 2p, and Mo 3d for MoCoNiS@NF. The spectra of Co 2p indicate two spectral peaks at ~780.3 and 796.3 eV with their neighboring shakeup satellite peaks, representing Co^{2+} from the Co $2p_{3/2}$ and Co $2p_{1/2}$ orbitals (Fig. 3**c**) [52, 53]. In the spectra of Ni 2p, the peaks located at 854.0 eV and 870.5 eV were identified as Ni^{2+}, and two peaks at 856.7 eV and 874.3 eV correspond to Ni^{3+}species in MoCoNiS@NF (Fig. 3**d**) [36,54,55]. Mo^{4+}, Mo^{5+}, and Mo^{6+}species were detected at around 230.5 eV, 231.2 eV, and 233.1 eV for Mo $3d_{5/2}$ and 233.5 eV, 234.2 eV, and 236.1 eV for Mo $3d_{3/2}$ (Fig. 3**e**). [56,57] The peaks at 162.6 eV and 164.0 eV of S 2p are resulting from S^{2-} and S_2^{2-} ligands in metal sulfides (**Figure S3b**) [58]. For FeCoNiS@NF, the XPS full-scan survey showed the presence of different elements in FeCoNiS@NF (**Figure S3c**). The corresponding high-resolution spectra indicated that Co, Ni, and S in FeCoNiS@NF

have similar properties as in MoCoNiS@NF (**Figure S3d-f**). Fig. 3**f** shows several peaks from 700 to 730 eV, which can be assigned to Fe $2p_{3/2}$ and Fe $2p_{1/2}$. The peaks showing at ~707.1 eV, 711.4 eV, and 714.0 eV with their shakeup satellite peaks indicated that iron has multiple oxidation states including Fe^{2+} and Fe^{3+} [59]. These characterization results proved that multiple-metal sulfides were successfully synthesized by an electrodeposition process, which is well consistent with the EDS and Raman observations.

3.2. Electrocatalytic water splitting

To evaluate the electrocatalytic performance of the metal sulfides for alkaline water-splitting reactions, the electrochemical activities of all the fabricated electrodes were examined in 1 M KOH solution. **Figure S4** presents the OER and HER activities of different metal sulfides evaluated by LSV. The measured potentials against RHE have been corrected with iR-compensation for the OER polarization curves in Fig. 4**a**. The polarization curve of NiS@NF showed a large oxidation peak at ~1.40 V (vs. RHE), resulting from the oxidation of its Ni species. Compared with bare Ni foam, NiS@NF showed much better OER electrocatalytic activity, requiring an overpotential of 363 mV at 50 mA cm^{-2}. This result suggested that nickel sulfides deposited by the electrodeposition technique were active towards OER. The oxidation peaks of Co and Ni species were observed at around 1.20 and 1.35 V from the LSV curve of CoNiS@NF. The shift of the Ni oxidation peak is probably due to the electronic structure and morphology change by introducing Co metal atoms in the bimetallic sulfides. Importantly, the designed CoNiS@NF exhibited enhanced OER performance at an overpotential of 340 mV at 50 mA cm^{-2}, demonstrating that CoNiS@NF has higher OER activity than NiS@NF. The enhancement in OER electrocatalytic activity could be attributed to the synergistic interface of cobalt-nickel sulfide in CoNiS@NF. Furthermore, the vertically oriented nanoflakes morphology provides more accessible active sites for interaction with electrolyte molecules during the water oxidation reactions. It should be noted here that the incorporation of Mo into cobalt-nickel sulfides neither reduces nor enhances the OER activity (MoCoNiS@NF), while it increases the HER activity in the alkaline medium, indicating the importance of Mo incorporation into the cobalt-nickel sulfides. Compared with other self-standing electrodes, the electrode based on FeCoNiS@NF possesses the best OER electrocatalytic activity with low overpotentials of 302 and 307 mV at 50 and 100 mA cm^{-2}, respectively (Fig. 4**b**). The excellent OER activity of FeCoNiS@NF could be ascribed to the synergistic coupling of multi-transition metals in their heterostructures. Furthermore, this electrode is very beneficial for the OER process because (1) the Ni foam substrate offers excellent electrical conductivity for electron transport and a large surface area for active materials; (2) the incorporation of iron into cobalt-nickel sulfides probably lowers the adsorption energy; (3) iron-cobalt-nickel sulfides provide abundant active sites for expediting the OER process. For comparison, commercial IrO_2 coated on Ni foam electrode was prepared and recorded its polarization curve in 1 M KOH for OER (**Figure S5a**). FeCoNiS@NF presented higher OER electrocatalytic activity than IrO_2@NF with the same mass loading, implying that multi-metal sulfides are competitive in OER and therefore it can be considered an efficient anode electrode in a large-scale alkaline electrolyzer. We also compared the OER performance of FeCoNiS@NF in 1 M KOH with other reported electrocatalysts, summarized in **Table S2**. The EIS results for the different electrodes were analyzed with the appropriate equivalent circuit as shown in **Figure S6**. The extracted various electrochemical kinetic parameters are presented in **Table S3**, where R_s, R_{ct}, and R_{int} represent the solution, charge transfer, and interfacial resistances, respectively [29]. Whereas C_{Chem} and C_{dl} are the interfacial chemical capacitance and double-layer capacitance, respectively [29]. As shown in Fig. 4**c**, EIS analysis was conducted to study the OER kinetics based on the charge-transfer resistance (R_{ct}). Metal sulfides deposited on Ni foam have much lower R_{ct} values than bare Ni foam, owing to the faster electron transport for oxygen evolution over metal sulfides. Compared with other electrodes, FeCoNiS@NF has the lowest R_{ct} value, probably due to the formation of iron-cobalt-nickel-sulfide heterostructure hybrids with high conductivity and electrochemical activity. This unique interface of FeCoNiS@NF could decrease the interface resistance and thus enhance OER performance. Fig. 4**d** presents the Tafel slopes of different electrodes, which are obtained from polarization curves. FeCoNiS@NF is found to have a small Tafel slope of 33 mV dec^{-1}, which is smaller than that of all other metal sulfide samples (106 mV dec^{-1} for NiS@NF, 62 mV dec^{-1} for CoNiS@NF and 61 mV dec^{-1} for MoCoNiS@NF). The Tafel slope of nickel sulfides was remarkably reduced by the incorporation of Co or Co/Fe or Co/Mo metal atoms, resulting in a much faster OER kinetics due to the regulation of electronic structure and adsorption energy for the oxygen intermediates. It is worth mentioning here that FeCoNiS@NF presents a much lower Tafel slope than other fabricated electrodes and also lower than recently reported efficient OER electrodes based on non-precious catalysts [60–62]. It strongly indicated that the energy-efficient electrodeposition process reported here is a promising method to produce trimetallic sulfides for the outstanding water oxidation reaction. The chronoamperometric technique was performed to study the electrocatalytic OER durability test of the FeCoNiS@NF. The potential remained constant for 24 h of continuous OER process (at 30 mA cm^{-2}), demonstrating the superior OER durability of this electrode (Fig. 4**e**).

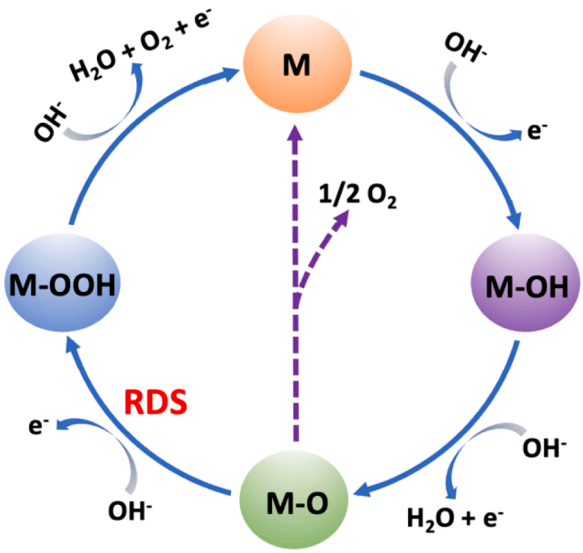

Fig. 5. OER mechanism in alkaline medium.

The possible mechanism for OER at the anode in the alkaline medium is presented in Fig. 5, which involves several steps. Here, M refers to the active sites on the catalyst surface. Generally, M-OH, M-O, and M-OOH reaction intermediates are generated during the OER process. Then, oxygen could be generated by the direct combination of two MO molecules or through M-OOH intermediates. It has been reported that the adsorption of OH^- and intermediates plays an essential role in the OER catalytic process of the electrode [63]. It is generally accepted that the Tafel slope value for any electrocatalysts/electrodes depends on the surface adsorption coverage of the reaction intermediates. Moreover, the Tafel slope value can determine the rate-limiting step in the multi-step electron transfer reactions on the surface of self-standing electrodes. For instance, the electrodes with high or low Tafel slope values have a rate-limiting step at the initial or end of OER cycles. The observed low change-transfer resistance and Tafel slope value of FeCoNiS@NF imply that it has faster reaction kinetics and a higher reaction rate of oxygen evolution compared to other electrodes. More importantly, the calculated Tafel slope value (33 mV dec^{-1}) indicates that the OER mechanism on the FeCoNiS@NF electrode surface occurs *via* M-OOH intermediates and predicts the generation of M-OOH

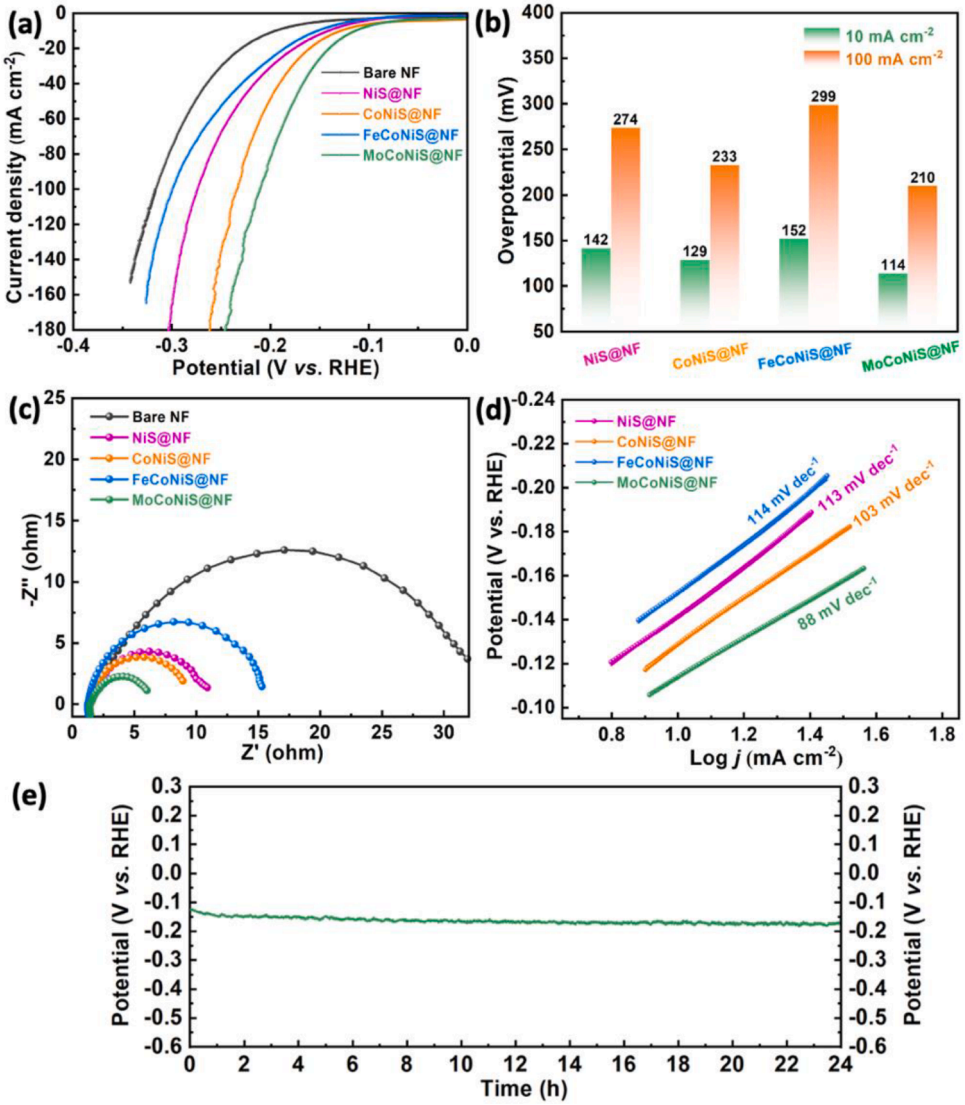

Fig. 6. Comparison of electrocatalytic HER activity of different electrodes. (a) LSV curves of several electrodes at a scan rate of 5 mV/s; (b) comparison of overpotentials versus different electrodes for HER (after iR-correction); (c) Nyquist plots obtained for various electrodes at a potential of −0.12 V (vs. RHE).; (d) Tafel plots of fabricated electrodes and (e) durability test of MoCoNiS@NF (without iR-correction).

intermediates as the rate-limiting step on FeCoNiS@NF electrode surface [64]. The excellent OER performance of FeCoNiS@NF might be because the adsorption of $OH^-$and intermediates on its surface is more favorable than that on other metal sulfide surfaces. Moreover, the incorporation of Fe could accelerate the OER process due to the synergistic interaction between different metals and the change in its electronic structures [63].

The HER performance of these self-supported metal sulfide electrodes was also analyzed in 1.0 M KOH solution. The corresponding LSV curves of different electrodes present a great difference in HER catalytic activities for different electrodes (Fig. 6**a**). As shown in Fig. 6**b**, MoCoNiS@NF only requires a low overpotential of 114 mV to achieve a current density of 10 mA cm^{-2}, revealing its excellent electrocatalytic activity for HER compared with different types of electrocatalysts (**Table S4**). The commercial Pt/C coated on Ni foam substrate with the same loading was also measured for comparison, which is shown in **Figure S5b**. The EIS analysis of different electrodes is shown in Fig. 6**c**, and the obtained various electrochemical kinetic parameters are presented in **Table S5**. Alike to OER, both R_{ct} and R_{int} values for the metal sulfides deposited on NF were much lower than bare NF due to the fabricated electrodes having high electrochemically active sites and surface areas for the water oxidation reaction. The obtained EIS results revealed that a rapid charge transfer process takes place during HER on the surface of CoNiS@NF and MoCoNiS@NF electrodes with electrolyte solution compared to other fabricated electrodes and bare NF. The Tafel plots for HER of different metal sulfide electrodes are presented in Fig. 6**d.** NiS@NF, CoNiS@NF, and FeCoNiS@NF exhibit relatively high Tafel slopes of 113, 103, and 114 mV dec^{-1}, respectively, while MoCoNiS@NF presents a small Tafel slope of 88 mV dec^{-1}. This observation indicates a faster HER reaction kinetics of MoCoNiS@NF due to the introduction of HER active Mo atoms in the cobalt-nickel sulfides, lowering the adsorption energy of the hydrogen. In the alkaline electrolyte solution, the HER mechanism possibly involves multiple steps as follows: (1) water dissociation and reactant adsorption (Volmer reaction: $M + H_2O + e^- \rightarrow M\text{–}H^* + OH^-$), (2) product desorption (Heyrovsky reaction: $M\text{–}H^* + H_2O + e^- \rightarrow H_2 + M + OH^-$), and/or (3) the chemical desorption (Tafel reaction: $2M\text{–}H^* \rightarrow H_2 + 2\ M$) [65]. M refers to the catalytic active sites and H* is the H atoms adsorbed on an electrocatalyst active site. The hydrogen evolution following a Volmer-Heyrovsky or Volmer-Tafel process depends on the structures and electronic properties of the electrocatalysts/electrodes. Several factors may contribute to the good HER activity of MoCoNiS@NF.

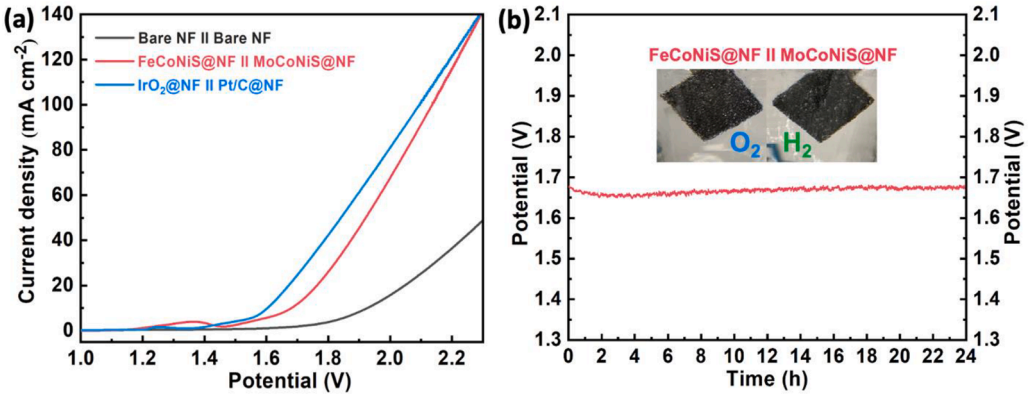

Fig. 7. (a) Overall water splitting performance of different pairs of electrodes in a two-electrode system. (b) Corresponding chronoamperometric response of FeCoNiS@NF II MoCoNiS@NF for stability (Inset: O_2 and H_2 bubbles released during water splitting).

Firstly, this electrode has high conductivity, enhancing electron transfer during the electrochemical reaction, resulting from the high metallic conductivity of metal sulfide heterostructures and the electrically conductive Ni foam substrate. Secondly, these metal sulfides have high intrinsic catalytic activity and offer abundant active sites for HER. Furthermore, the incorporation of Mo probably enhances the water reduction and reactant adsorption, making the HER process more favorable. Finally, the synergistic effect of the Mo, Co, and Ni trimetallic sulfides exerts a positive effect on HER activity. It should be noted that FeCoNiS@NF has poor HER activity, which is worse than NiS@NF. The main reason probably is the high adsorption energy of FeCoNiS@NF for water, which is relatively unfavorable for the first step of the HER process, which is also confirmed by the observed Tafel slope value. The electrochemical HER durability of the MoCoNiS@NF heterostructures was also performed by the chronopotentiometry technique. This MoCoNiS@NF electrode can maintain a relatively consistent operating potential at 10 mA cm^{-2} for 24 h, demonstrating the acceptable durability of this electrode for the HER process (Fig. 6**e**).

To evaluate the possibility of utilizing these hybrids of self-supported trimetallic sulfide electrodes for large-scale hydrogen production in an alkaline medium, FeCoNiS@NF as anode and MoCoNiS@NF as cathode were utilized to construct a two-electrode system for overall electrochemical water electrolysis. Fig. 7**a** presents the corresponding LSV curves of three systems evaluated in 1 M KOH with a scan rate of 5 mV s^{-1}. FeCoNiS@NF II MoCoNiS@NF shows much higher electrocatalytic activity than bare Ni foam, requiring 1.68 V to deliver a current density of 10 mA cm^{-2}. For comparison, IrO_2@NF and Pt/C@NF served as the anode and cathode under the same conditions, respectively. The long-time durability test of FeCoNiS@NF II MoCoNiS@NF for overall water electrolysis is performed by applying a continuous current density (10 mA cm^{-2}), as indicated in Fig. 7**b**. The generation of O_2 and H_2 bubbles was observed during water splitting (Fig. 7**b inset**). The voltage of this two-electrode system remains stable for at least 24 h of testing.

Based on the experimental results, this study presents several improvements compared with the published work. Firstly, the electrochemical activity is a key factor in evaluating an electrocatalyst for OER/HER. FeCoNiS@NF and MoCoNiS@NF exhibit high catalytic OER and HER performance compared with similar electrocatalysts [14,34,66,67]. Secondly, we proved that heterostructure interfaces of metal sulfides were largely responsible for the OER and HER activities. These findings suggest that metal sulfides with rational design could be promising electrocatalysts to alternate noble metal-based electrocatalysts for overall water splitting. In addition, we provide the EIS simulation data of different metal sulfides for OER and HER, which will help to understand the working mechanisms behind the electrochemical behaviors of the electrocatalysts. Finally, FeCoNiS@NF and MoCoNiS@NF as asymmetric electrodes could be assembled into an alkaline water electrolysis system, offering another option to develop efficient electrolyzers for hydrogen production.

4. Conclusions

In this study, we demonstrated monometallic, bimetallic, and trimetallic sulfides with varying OER and HER activities. Notably, FeCoNiS@NF has the advantage of a low overpotential (302 mV at 50 mA cm^{-2}) for OER while MoCoNiS@NF can provide a current density of 10 mA cm^{-2} at an overpotential of 114 mV for HER. The outstanding OER activity of FeCoNiS@NF and HER activity of MoCoNiS@NF are attributed to not only the diversity of metal sulfide compositions, electronic interaction, and hybrid structures, but also the optimization of charge-transfer, catalytic active sites, and synergistically coupling of heterostructure interfaces of multi-metal sulfides. In addition, we proved that FeCoNiS@NF and MoCoNiS@NF have fast reaction rates toward OER and HER, respectively, from EIS and Tafel slope analysis. This work provides new perspectives for the future design of self-supported metal sulfide electrodes for water-splitting via rational engineering of nanostructures and interfaces.

Declaration of Competing Interest

The authors declare that they have no known competing financial interests or personal relationships that could have appeared to influence the work reported in this paper.

Credit authorship contribution statement

Rong He designed and performed the experiments, wrote the draft, analyzed the data and; Pitchai Thangasamy helped the experiments and electrochemical testing; Junlin Wu, Kunpeng Yu, Xiaolu Yu and Wei Tang did materials characterizations including HRTEM, XPS and SEM; Devon Quiroz and Deema Alyones helped with the material synthesis. Zheng Chen, Hongmei Luo and Meng Zhou proposed the research direction, oversaw the project, and provided funding supports. All authors checked the manuscript and agreed with this statement.

Acknowledgments

The work is funded by the National Science Foundation OIA-2119688, MRI-2215982 and MRI-2216473.

Supplementary materials

Supplementary material associated with this article can be found, in the online version, at doi:10.1016/j.electacta.2023.143342.

References

[1] J. Chow, R.J. Kopp, P.R. Portney, Energy resources and global development, Science 302 (2003) 1528–1531.
[2] A.M. Oliveira, R.R. Beswick, Y. Yan, A green hydrogen economy for a renewable energy society, Curr. Opin. Chem. Eng. 33 (2021), 100701.
[3] I. Dincer, Green methods for hydrogen production, Int. J. Hydrogen Energy 37 (2012) 1954–1971.
[4] P. Thangasamy, R. He, H. Randriamahazaka, X. Chen, Y. Zhang, H. Luo, H. Wang, M. Zhou, Collectively exhaustive electrochemical hydrogen evolution reaction of polymorphic cobalt selenides derived from organic surfactants modified Co-MOFs, Appl. Catal., B 325 (2023), 122367.
[5] C. Hu, L. Zhang, J. Gong, Recent progress made in the mechanism comprehension and design of electrocatalysts for alkaline water splitting, Energy Environ. Sci. 12 (2019) 2620–2645.
[6] B. Sarkar, B.K. Barman, K.K. Nanda, Non-precious bimetallic CoCr nanostructures entrapped in bamboo-like nitrogen-doped graphene tube as a robust bifunctional electrocatalyst for total water splitting, ACS Appl. Energy Mater. 1 (2018) 1116–1126.
[7] S. Li, X. Hao, A. Abudula, G. Guan, Nanostructured Co-based bifunctional electrocatalysts for energy conversion and storage: current status and perspectives, J. Mater. Chem. A 7 (2019) 18674–18707.
[8] C. Li, J.B. Baek, Recent advances in noble metal (Pt, Ru, and Ir)-based electrocatalysts for efficient hydrogen evolution reaction, ACS Omega 5 (2020) 31–40.
[9] T. Audichon, T.W. Napporn, C. Canaff, C. Morais, C. Comminges, K.B. Kokoh, IrO2 coated on RuO2 as efficient and stable electroactive nanocatalysts for electrochemical water splitting, J. Phys. Chem. C 120 (2016) 2562–2573.
[10] Z. Pu, I.S. Amiinu, Z. Kou, W. Li, S. Mu, RuP(2) -based catalysts with platinum-like activity and higher durability for the hydrogen evolution reaction at all pH values, Angew. Chem. Int. Ed. 56 (2017) 11559–11564.
[11] K. Park, S. Choi, J. Kwon, J. Kim, S. Jo, K. Lee, H.B. Park, H. Han, U. Paik, T. Song, Two-dimensional hierarchical CoTe/NiFe layered double hydroxide heterostructure for high-performance electrocatalytic water oxidation, ACS Appl. Energy Mater. 6 (2023) 3432–3441.
[12] N.T. Suen, S.F. Hung, Q. Quan, N. Zhang, Y.J. Xu, H.M. Chen, Electrocatalysis for the oxygen evolution reaction: recent development and future perspectives, Chem. Soc. Rev. 46 (2017) 337–365.
[13] Z.Y. Yu, Y. Duan, X.Y. Feng, X. Yu, M.R. Gao, S.H. Yu, Clean and affordable hydrogen fuel from alkaline water splitting: past, recent progress, and future prospects, Adv. Mater. 33 (2021), e2007100.
[14] R. Zahra, E. Pervaiz, M.M. Baig, O. Rabi, Three-dimensional hierarchical flowers-like cobalt-nickel sulfide constructed on graphitic carbon nitride: bifunctional non-noble electrocatalyst for overall water splitting, Electrochim. Acta 418 (2022), 140346.
[15] J.-H. Yoon, Y.A. Kumar, S. Sambasivam, S.A. Hira, T.N.V. Krishna, K. Zeb, W. Uddin, K.D. Kumar, I.M. Obaidat, S. Kim, H.-J. Kim, Highly efficient copper-cobalt sulfide nano-reeds array with simplistic fabrication strategy for battery-type supercapacitors, J. Energy Storage 32 (2020), 101988.
[16] Y.A. Kumar, G. Mani, M.R. Pallavolu, S. Sambasivam, R.R. Nallapureddy, M. Selvaraj, M. Alfakeer, A.A.A. Bahajjaj, M. Ouladsmane, S.S. Rao, S. Ramakrishna, Facile synthesis of efficient construction of tungsten disulfide/iron cobaltite nanocomposite grown on nickel foam as a battery-type energy material for electrochemical supercapacitors with superior performance, J. Colloid Interface Sci. 609 (2022) 434–446.
[17] S. Yuan, X. Duan, J. Liu, Y. Ye, F. Lv, T. Liu, Q. Wang, X. Zhang, Recent progress on transition metal oxides as advanced materials for energy conversion and storage, Energy Storage Mater 42 (2021) 317–369.
[18] F. Lu, M. Zhou, Y. Zhou, X. Zeng, First-row transition metal based catalysts for the oxygen evolution reaction under alkaline conditions: basic principles and recent advances, Small 13 (2017), 1701931.
[19] K. Zhang, R. Zou, Advanced transition metal-based OER electrocatalysts: current status, opportunities, and challenges, Small 17 (2021), e2100129.
[20] B. You, Y. Zhang, Y. Jiao, K. Davey, S.Z. Qiao, Negative charging of transition-metal phosphides via strong electronic coupling for destabilization of alkaline water, Angew. Chem. Int. Ed. 58 (2019) 11796–11800.
[21] P. Wang, B. Wang, Interface engineering of binder-free earth-abundant electrocatalysts for efficient advanced energy conversion, ChemSusChem 13 (2020) 4795–4811.
[22] J. Kwon, H. Han, S. Choi, K. Park, S. Jo, U. Paik, T. Song, Current status of self-supported catalysts for robust and efficient water splitting for commercial electrolyzer, ChemCatChem 11 (2019) 5898–5912.
[23] N. Jiang, B. You, M. Sheng, Y. Sun, Electrodeposited cobalt-phosphorous-derived films as competent bifunctional catalysts for overall water splitting, Angew. Chem. Int. Ed. 54 (2015) 6251–6254.
[24] Q. Zhang, Y. Wang, Y. Wang, A.M. Al-Enizi, A.A. Elzatahry, G. Zheng, Myriophyllum-like hierarchical TiN@Ni3N nanowire arrays for bifunctional water splitting catalysts, J. Mater. Chem. A 4 (2016) 5713–5718.
[25] P. Wang, J. Qi, X. Chen, C. Li, W. Li, T. Wang, C. Liang, Three-dimensional heterostructured NiCoP@NiMn-layered double hydroxide arrays supported on Ni foam as a bifunctional electrocatalyst for overall water splitting, ACS Appl. Mater. Interfaces 12 (2020) 4385–4395.
[26] J. Joo, T. Kim, J. Lee, S.I. Choi, K. Lee, Morphology-controlled metal sulfides and phosphides for electrochemical water splitting, Adv. Mater. 31 (2019), e1806682.
[27] S. Zhang, Y. Li, H. Zhu, S. Lu, P. Ma, W. Dong, F. Duan, M. Chen, M. Du, Understanding the role of nanoscale heterointerfaces in core/shell structures for water splitting: covalent bonding interaction boosts the activity of binary transition-metal sulfides, ACS Appl. Mater. Interfaces 12 (2020) 6250–6261.
[28] R. Biswas, I. Ahmed, P. Manna, P. Mahata, R.S. Dhayal, A. Singh, J. Lahtinen, K. K. Haldar, Facile fabrication of Ni(9) S(8) /Ag(2) S intertwined structures for oxygen and hydrogen evolution reactions, Chempluschem 88 (2023), e202200320.
[29] P. Thangasamy, S. Oh, S. Nam, H. Randriamahazaka, I.K. Oh, Ferrocene-incorporated cobalt sulfide nanoarchitecture for superior oxygen evolution reaction, Small 16 (2020), 2001665.
[30] W. Tang, J. Jian, G. Chen, W. Bian, J. Yu, H. Wang, M. Zhou, D. Ding, H. Luo, Carbon nanotube supported amorphous MoS2 via microwave heating synthesis for enhanced performance of hydrogen evolution reaction, Energy Mater. Adv. 2021 (2021) 1–8.
[31] R. He, Q. Sun, P. Thangasamy, X. Chen, Y. Zhang, H. Wang, H. Luo, X.-D. Zhou, M. Zhou, Accelerate oxygen evolution reaction by adding chemical mediator and utilizing solar energy, Int. J. Hydrogen Energy 48 (2023) 8898–8908.
[32] Z. Huang, Z. Yang, M.Z. Hussain, B. Chen, Q. Jia, Y. Zhu, Y. Xia, Polyoxometallates@zeolitic-imidazolate-framework derived bimetallic tungsten-cobalt sulfide/porous carbon nanocomposites as efficient bifunctional electrocatalysts for hydrogen and oxygen evolution, Electrochim. Acta 330 (2020), 135335.
[33] M. Wang, L. Zhang, Y. He, H. Zhu, Recent advances in transition-metal-sulfide-based bifunctional electrocatalysts for overall water splitting, J. Mater. Chem. A 9 (2021) 5320–5363.
[34] K.S. Bhat, H.S. Nagaraja, In situ synthesis of copper sulfide-nickel sulfide arrays on three-dimensional nickel foam for overall water splitting, ChemistrySelect 5 (2020) 2455–2464.
[35] X. Zheng, X. Han, Y. Zhang, J. Wang, C. Zhong, Y. Deng, W. Hu, Controllable synthesis of nickel sulfide nanocatalysts and their phase-dependent performance for overall water splitting, Nanoscale 11 (2019) 5646–5654.
[36] D. Chinnadurai, R. Rajendiran, P. Kandasamy, Bimetallic copper nickel sulfide electrocatalyst by one step chemical bath deposition for efficient and stable overall water splitting applications, J. Colloid Interface Sci. 606 (2022) 101–112.
[37] K. Xiao, J.X. Wei, W.K. Han, Z.Q. Liu, Bimetallic sulfide interfaces: promoting destabilization of water molecules for overall water splitting, J. Power Sources 487 (2021), 229408.
[38] Y.A. Kumar, B.A. Al-Asbahi, M.R. Pallavolu, S.S. Rao, R.R. Nallapureddy, S. Ramakrishna, Multiple structural defects in poor crystalline nickel-doped tungsten disulfide nanorods remarkably enhance supercapacitive performance, Int. J. Energy Res. 46 (2022) 14227–14239.
[39] Y.A. Kumar, H.T. Das, P.R. Guddeti, R.R. Nallapureddy, M.R. Pallavolu, S. Alzahmi, I.M. Obaidat, Self-supported Co(3)O(4)@Mo-Co(3)O(4) needle-like nanosheet heterostructured architectures of battery-type electrodes for high-performance asymmetric supercapacitors, Nanomater. 12 (2022) 2330.
[40] C. Miao, X. Zheng, J. Sun, H. Wang, J. Qiao, N. Han, S. Wang, W. Gao, X. Liu, Z.-x. Yang, Facile electrodeposition of amorphous nickel/nickel sulfide composite films for high-efficiency hydrogen evolution reaction, ACS Appl. Energy Mater. 4 (2021) 927–933.
[41] Y.A. Kumar, K.D. Kumar, H.-J. Kim, Facile preparation of a highly efficient NiZn(2) O(4)-NiO nanoflower composite grown on Ni foam as an advanced battery-type electrode material for high-performance electrochemical supercapacitors, Dalton Trans 49 (2020) 3622–3629.
[42] S. Shit, S. Bolar, N.C. Murmu, T. Kuila, Tailoring the bifunctional electrocatalytic activity of electrodeposited molybdenum sulfide/iron oxide heterostructure to achieve excellent overall water splitting, Chem. Eng. J. 417 (2021), 129333.
[43] B. Wang, S. Jiao, Z. Wang, M. Lu, D. Chen, Y. Kang, G. Pang, S. Feng, Rational design of NiFe LDH@ Ni 3N nano/microsheet arrays as a bifunctional electrocatalyst for overall water splitting, J. Mater. Chem. A 8 (2020) 17202–17211.
[44] Y.A. Kumar, K.D. Kumar, H.-J. Kim, Reagents assisted ZnCo2O4 nanomaterial for supercapacitor application, Electrochim. Acta 330 (2020), 135261.
[45] Y.A. Kumar, S. Sambasivam, S.A. Hira, K. Zeb, W. Uddin, T.N.V. Krishna, K. D. Kumar, I.M. Obaidat, H.-J. Kim, Boosting the energy density of highly efficient flexible hybrid supercapacitors via selective integration of hierarchical nanostructured energy materials, Electrochim. Acta 364 (2020), 137318.
[46] P. Thangasamy, R. He, X. Chen, K. Yu, H. Randriamahazaka, Z. Chen, H. Luo, X. D. Zhou, M. Zhou, Organic-inorganic hybrid crystal-assisted etching of nickel foam for the collectively exhaustive electrochemical performance of oxygen evolution reaction, Chem. Eur. J 29 (2023), e202301469.
[47] N. Feng, D. Hu, P. Wang, X. Sun, X. Li, D. He, Growth of nanostructured nickel sulfide films on Ni foam as high-performance cathodes for lithium ion batteries, Phys. Chem. Chem. Phys. 15 (2013) 9924–9930.
[48] S.G. Mohamed, I. Hussain, J.J. Shim, One-step synthesis of hollow C-NiCo(2)S(4) nanostructures for high-performance supercapacitor electrodes, Nanoscale 10 (2018) 6620–6628.
[49] P. Wen, M. Fan, D. Yang, Y. Wang, H. Cheng, J. Wang, An asymmetric supercapacitor with ultrahigh energy density based on nickle cobalt sulfide nanocluster anchoring multi-wall carbon nanotubes hybrid, J. Power Sources 320 (2016) 28–36.
[50] Y. Gao, W. Liao, W. Wang, X. Zuo, Q. Yang, H. Tang, S. Jin, G. Li, FeS2/FeCoS2 nanoparticles/reduced graphene oxide interfacial composite structure as highly reactive counter electrodes in dye-sensitized solar cells, J. Mater. Sci.: Mater. Electron. 32 (2021) 8226–8236.
[51] C.V.M. Inocêncio, J. Rousseau, N. Guignard, C. Canaff, S. Morisset, C. Comminges, C. Morais, K.B. Kokoh, Taking advantage of teamwork: unsupported cobalt molybdenum sulfide as an active HER electrocatalyst in alkaline media, J. Electrochem. Soc. 169 (2022), 054524.

[52] D. Wu, Y. Wei, X. Ren, X. Ji, Y. Liu, X. Guo, Z. Liu, A.M. Asiri, Q. Wei, X. Sun, Co (OH)(2) nanoparticle-encapsulating conductive nanowires array: room-temperature electrochemical preparation for high-performance water oxidation electrocatalysis, Adv. Mater. 30 (2018), 1705366.
[53] D.K. Kumar, Y.A. Kumar, H.-J. Kim, Hierarchical NiCo2S4 nanostructure as highly efficient electrode material for high-performance supercapacitor applications, J. Energy Storage 31 (2020), 101619.
[54] B. Ma, X. Guo, X. Zhang, Y. Chen, X. Fan, Y. Li, F. Zhang, G. Zhang, W. Peng, Intercalated graphite between Ni foam and Ni3S2 nanocrystals for the activity promotion in overall water splitting, Energy Technol. 7 (2019), 1900063.
[55] Y.A. Kumar, H.-J. Kim, Wearable super-high specific performance supercapacitors using a honeycomb with folded silk-like composite of NiCo(2)O(4) nanoplates decorated with NiMoO(4) honeycombs on nickel foam, Dalton Trans. 47 (2018) 15545–15554.
[56] P. Kumar, M. Singh, G.B. Reddy, Oxidation of core–shell MoO2–MoS2nanoflakes in different O2ambience, Mater. Res. Express 4 (2017), 036405.
[57] L. Lin, Z.K. Yang, Y.F. Jiang, A.W. Xu, Nonprecious bimetallic (Fe,Mo)–N/C catalyst for efficient oxygen reduction reaction, ACS Catal 6 (2016) 4449–4454.
[58] D. Dinda, M.E. Ahmed, S. Mandal, B. Mondal, S.K. Saha, Amorphous molybdenum sulfide quantum dots: an efficient hydrogen evolution electrocatalyst in neutral medium, J. Mater. Chem. A 4 (2016) 15486–15493.
[59] L. Li, P. Ma, S. Hussain, L. Jia, D. Lin, X. Yin, Y. Lin, Z. Cheng, L. Wang, FeS2/carbon hybrids on carbon cloth: a highly efficient and stable counter electrode for dye-sensitized solar cells, Sustainable Energy Fuels 3 (2019) 1749–1756.
[60] G. Wang, S. Yang, M. Lu, B. Hua, Z. Zhang, J. Kang, W. Tang, H. Wei, L. Cui, X. Chen, Sulfonated polybenzimidazole engineering defect-induced N, S-codoped carbon-supported Co3C hybrid composite as high-efficiency electrocatalyst for oxygen evolution reaction, Electrochim. Acta 443 (2023), 141939.
[61] K. Bera, A. Karmakar, S. Kumaravel, S. Sam Sankar, R. Madhu, N.D. H, S. Nagappan, S. Kundu, Vanadium-doped nickel cobalt layered double hydroxide: a high-performance oxygen evolution reaction electrocatalyst in alkaline medium, Inorg. Chem. 61 (2022) 4502–4512.
[62] A.S. Abu Hatab, Y.H. Ahmad, M. Ibrahim, A. Elsafi Ahmed, M.B. Abdul Rahman, S. Y. Al-Qaradawi, MOF-derived cobalt@mesoporous carbon as electrocatalysts for oxygen evolution reaction: impact of organic linker, Langmuir 39 (2023) 1123–1134.
[63] C. Feng, M.B. Faheem, J. Fu, Y. Xiao, C. Li, Y. Li, Fe-Based Electrocatalysts for Oxygen Evolution Reaction: progress and Perspectives, ACS Catal 10 (2020) 4019–4047.
[64] Q. Liu, H. Zhao, M. Jiang, Q. Kang, W. Zhou, P. Wang, F. Zhou, Boron enhances oxygen evolution reaction activity over Ni foam-supported iron boride nanowires, J. Mater. Chem. A 8 (2020) 13638–13645.
[65] N. Mahmood, Y. Yao, J.W. Zhang, L. Pan, X. Zhang, J.J. Zou, Electrocatalysts for hydrogen evolution in alkaline electrolytes: mechanisms, challenges, and prospective solutions, Adv. Sci. 5 (2018), 1700464.
[66] J.-H. Yang, X. Xu, M. Chen, D. Yang, H. Lu, Y. Sun, C. Shao, Q. Song, J. Zhang, L. Gao, Y. Zhang, Morphology-controllable nanocrystal β-Ni (OH) 2/NF designed by hydrothermal etching method as high-efficiency electrocatalyst for overall water splitting, J. Electroanal. Chem. 882 (2021), 115035.
[67] Z. Zhu, H. Yin, C.T. He, M. Al-Mamun, P. Liu, L. Jiang, Y. Zhao, Y. Wang, H. G. Yang, Z. Tang, D. Wang, X.M. Chen, H. Zhao, Ultrathin transition metal dichalcogenide/3d metal hydroxide hybridized nanosheets to enhance hydrogen evolution activity, Adv. Mater. 30 (2018), e1801171.